PIER C

(Received 20 September 2024, Accepted 16 October 2024, Scheduled 25 October 2024)

Multi Resonant Gap-Coupled Designs of E-Shape Microstrip Antenna for Wideband Response

Venkata A. P. Chavali and Amit A. Deshmukh*

EXTC, SVKM's D J Sanghvi CoE, Mumbai, India

ABSTRACT: The wideband gap-coupled configuration of an E-shape microstrip antenna, with two C-shape microstrip patches and loaded with a parasitic printed rectangular loop element, is proposed. In 1200 MHz frequency range and on a substrate thickness of $0.11\lambda_g$, with an optimum inter-spacing between the frequencies of TM_{10} and TM_{02} resonant modes of the rectangular patch along with TM_{20} resonant mode frequencies on the parasitic C-shape and printed rectangular loop element, the maximum reflection coefficient bandwidth of 945 MHz (68.11%) is achieved. The gap-coupled antenna offers broadside radiation characteristics across the complete bandwidth with a peak broadside gain of 9 dBi. Design methodology to realize wideband gap-coupled configuration in different frequency ranges is presented which yields similar result. The antenna response is experimentally verified which yields close agreement against the simulated result.

1. INTRODUCTION

Owing to the numerous advantages like low profile planar configuration, microstrip antenna (MSA) finds wide applications in wireless systems [1]. In the initial days, MSAs were considered as a narrow bandwidth (BW) and smaller gain elements [1], but over the last four–five decades different techniques have been evolved to enhance the above-mentioned MSA characteristics. A basic technique that achieves BW increment is a modified feed design on a thicker substrate [2-4]. Amongst various modified feed techniques, proximity feeding is the simplest one to be used. Another relatively simple technique that achieves a BW and gain increment is the multi-resonator gap-coupled design, in which parasitic patches of unequal dimensions are coupled to the fed patch [5–8]. However, this technique increases the antenna dimensions. By employing a dual edge shorted patch or using the combination of gap-coupled shorted patches or shorted patch combined with a differential feeding, wider BW designs are obtained [9–13]. To enhance the BW, shorted microstrip line feeding technique has also been used which provides a second order mode frequency suppression [14]. Amongst the different feeding techniques realized in MSA, aperture coupling yields maximum BW [1]. Using the same, wideband gap-coupled design of rectangular patches is presented in [15] that employs a U-shape feeding stub. A balance differential feeding technique yields BW improvement as discussed for the gap-coupled patches presented in [16]. However, differential feed requires a power divider to provide equal amplitude anti-parallel signals. By employing the combination of multiple patches in the gap-coupled and stacked layer wideband high gain antennas are obtained [1, 17]. They provide the gain larger than 10 dBi but requires larger antenna volume. Modified shape design employing a rectangular patch is discussed in [18] which provides 5% BW on a thinner substrate. By optimally utilizing the vacant space around the fed patch, wideband gap-coupled designs are reported [19–22, 32]. In these designs, the addition of every parasitic resonator around the fed patch adds to the BW but at the cost of increment in the patch size. By cutting the resonant slots inside the MSA fed using a coaxial or differential feed, or a differential fed MSA employing the combinations of slots and shorting post, wider BW designs are reported [23–29]. The resonant slots cut wideband design requires a thicker substrate. A design of slots cut MSA is reported in [30] which achieves a wideband response on a thinner substrate. By employing a modified ground plane profile in the form of slot or patch, wider BW designs are realized [31]. Thus, amongst various wideband techniques, gap-coupling method is the simplest of all. The resonant slots cut or modified ground plane designs maintain the low profile nature of the antenna, but they are complex in design. The later has smaller gain attributed to the modified ground plane profile. In gap-coupled MSAs, when empty space around fed patch is used, achieved BW is more than 50%, but for further increment in the BW when additional resonators are employed, the antenna size increases.

In this paper, a multi-resonator gap-coupled design of the E-shape MSA with two parasitic C-shape MSAs and loaded with a printed rectangular loop resonator is presented for a wideband response. The configurations are presented on a suspended FR4 substrate of thickness $\sim 0.11\lambda_g$, in 1200 MHz frequency band. Initially proximity fed design of a Rectangular Microstrip Antenna (RMSA) is discussed that achieves simulated impedance BW of 428 MHz (33.46%) with a broadside gain larger than 7 dBi. An increase in the BW of RMSA is achieved by gap-coupling the RMSA with two C-shape MSAs those were placed in the adjoining area of the fed RMSA. This gap-coupled design achieves reflection coefficient $(S_{11}) \leq -10$ dB BW of 743 MHz (57.31%) with a peak broadside gain of 8 dBi. To

* Corresponding author: Amit A. Deshmukh (amitdeshmukh76@gmail.com).

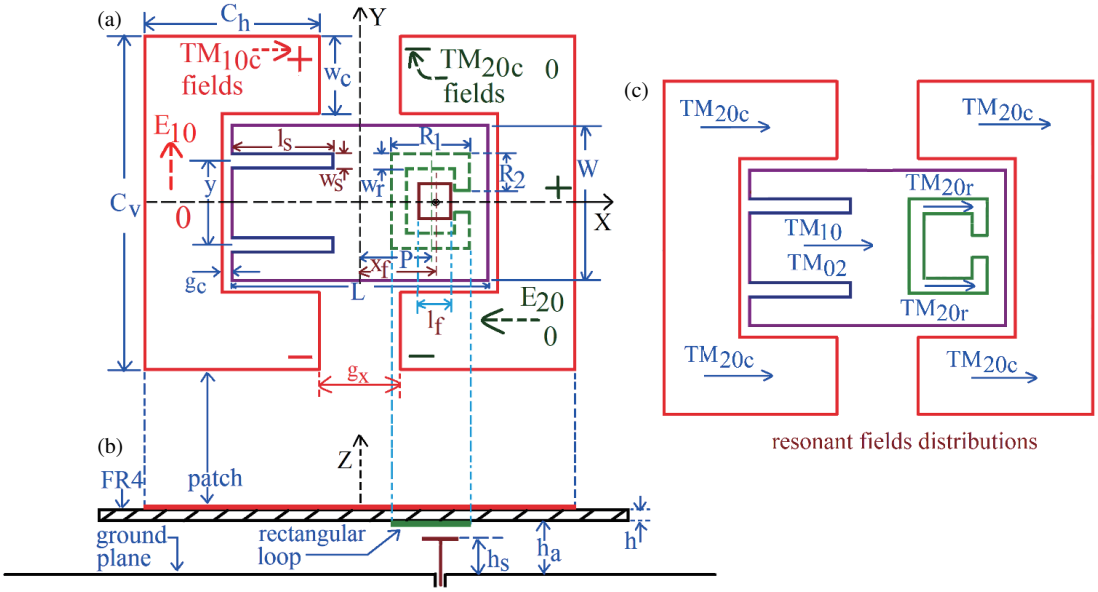

FIGURE 1. (a), (b) Proximity fed E-shape MSA gap-coupled with C-shape MSAs and loaded with printed rectangular loop resonator, (c) various resonant mode directions on the gap-coupled antenna.

further increase the BW, additional resonators were not gap-coupled to the fed patch, but first the pair of slots were embedded on the fed RMSA leading to E-shape design, which was further loaded with a printed rectangular loop resonator lying beneath the fed E-shape MSA. The gap-coupled design of E-shape MSA with two C-shape patches yields simulated BW of 902 MHz (66.13%) whereas the same gap-coupled configuration when being loaded with printed rectangular loop resonator below the E-shape patch yields simulated BW of 945 MHz (68.11%). Both these antennas yield broadside radiation pattern with a peak gain of 9 dBi. In both the designs, additional resonators were not externally added but placed below the patch or realized within the fed patch itself. Hence, the gap-coupled configuration achieves substantial BW improvement without further increment in the size of initial gap-coupled design. To highlight the technical novelty in the proposed study, detailed comparison against the reported wideband configurations is provided ahead in the paper. It shows that in terms of antenna volume, gain and S_{11} BW put together, the proposed design achieves an optimum performance. A resonant length formulation and subsequent design methodology to achieve a similar wideband antenna as per the given frequency spectrum is presented, which yields similar result. The antenna proposed in this work is initially optimized using CST software [33], followed by the experimental verifications carried out inside the antenna laboratory, using high frequency instruments namely, ZVH-8, SMB 100A and FSC 6.

2. MULTI-RESONATOR GAP-COUPLED VARIATIONS OF E-SHAPE MSA

The gap-coupled design of proximity fed E-shape MSA with two C-shape MSAs and loaded with a printed rectangular loop resonator located beneath the E-shape patch is shown in Figs. 1(a) and (b). The design is initiated with the proximity fed RMSA of length L and width W, fabricated on an FR4 substrate ($\varepsilon_r = 4.3$, $h = 0.16$ cm) and suspended above the ground plane using an air gap thickness of h_a cm.

The RMSA length is calculated such that for a total substrate thickness of 2.56 cm ($h_a = 2.4$ cm), TM_{10} mode frequency is 1200 MHz, thereby realizing electrical thickness of $\sim 0.1\lambda_g$. For these substrate parameters, RMSA length is found to be $L = 8.6$ cm. To realize a smaller size, patch width is selected as $W = 4.5$ cm. A square proximity strip of length L_f is placed at a distance of x_f from the patch center and at a thickness of h_s cm above the ground plane. This proximity feed position only excites TM_{10} mode on the patch. By optimizing strip parameters, RMSA is optimized for the wideband response. For antenna parameters as $L = 8.6$, $W = 4.5$, $h_a = 2.4$, $h_s = 2.3$, $x_f = 1.7$, $L_f = 1.3$ cm, simulated and measured S_{11} BWs are 428 MHz (33.43%) and 427 MHz (33.56%), respectively as shown in Fig. 2(a). The antenna offers broadside radiation pattern over the S_{11} BW with a peak gain of larger than 7 dBi.

To increase the BW, additional resonators are added in the structure. Gap-coupling parasitic C-shape patches with the proximity fed RMSA add resonant modes in the structure to achieve increase in the BW, as mentioned in Fig. 1(a). The C-shape patches are chosen as they occupy the vacant space around the proximity fed RMSA. Further, the resonant field distribution for C-shape MSA at first two modes is provided in Fig. 1(a). The fundamental TM_{10} mode in C-shape patch exhibits half wavelength variation along the C-shape length. With this field distribution, the E-plane (E_{10}) is directed along y-axis as shown in Fig. 1(a). At TM_{10} mode in the proximity fed RMSA, E-plane is present along the horizontal axis as shown in Figs. 1(a) and (c). With this, two E-planes are orthogonal and thus cannot provide wideband linearly polarized (LP) response. At second order mode in C-shape patch, the field shows

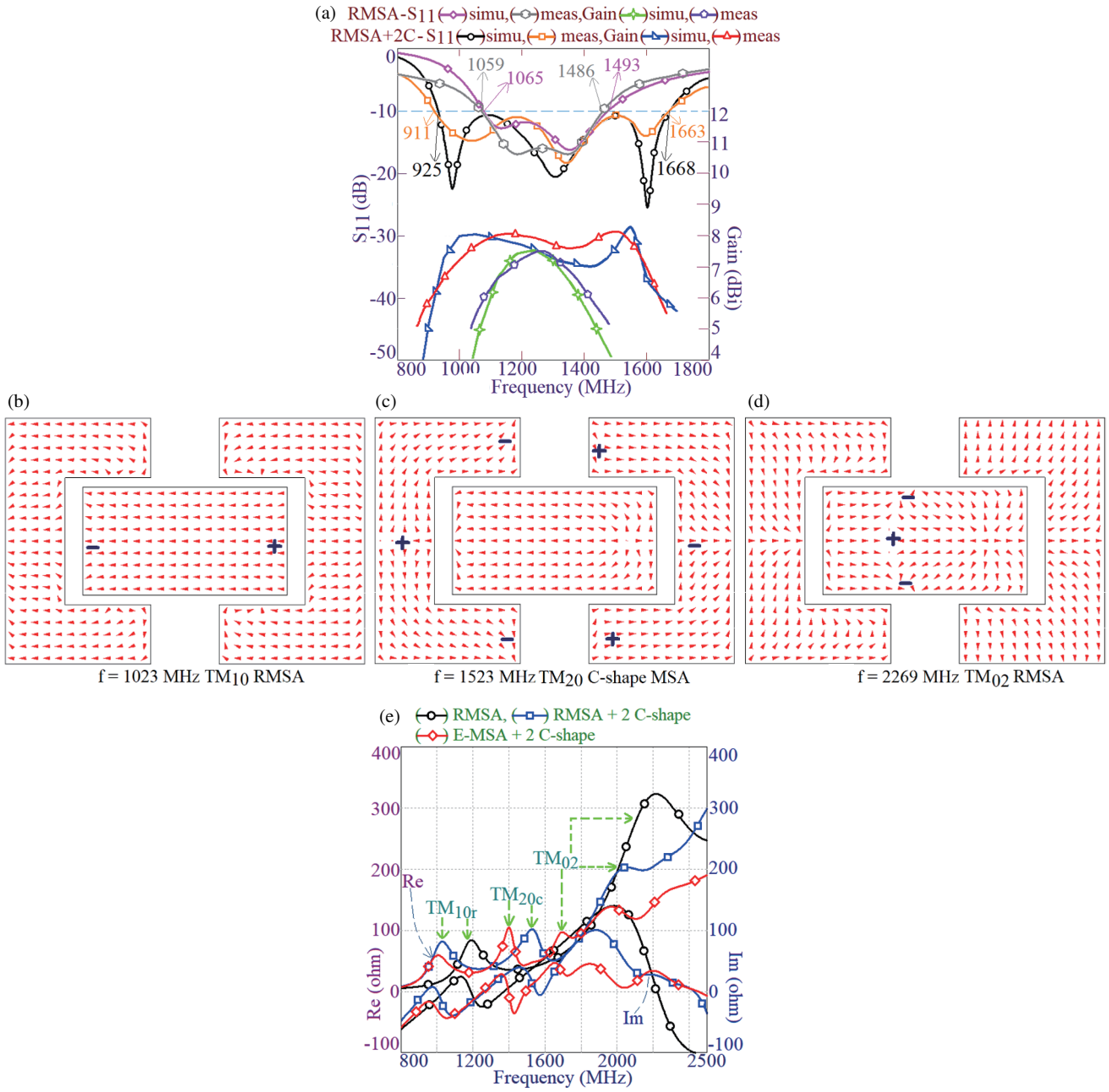

FIGURE 2. (a) S_{11} BW and gain plots for gap-coupled variations of proximity fed RMSA with C-shape MSAs, (b)–(d) vector surface current distribution at observed resonant modes for the gap-coupled design, and (e) resonance curve plots.

two half wavelength variation along C-shape patch length, and hence E-plane at the same is along the horizontal axis as shown in Figs. 1(a) and (c). For this mode, E-plane on the fed and parasitic patches are in the same direction, and thus the gap-coupling between them will provide wider BW LP response. Therefore, the wideband configuration with a gap-coupling of TM_{10} mode on RMSA and TM_{20} mode on C-shape MSA is presented. To achieve a wider BW, parametric variation for C-shape MSA length C_h, with $C_v = 10.3$, $W_c = 2.5$ cm, is carried out. The variations in C_h directly alters the resonance frequency of TM_{20} mode and tunes it with respect to TM_{10} mode frequency on RMSA which yields wider BW. Since this parametric optimization is similar to any gap-coupled design of two microstrip resonators, relevant resonance curve plots showing the variation in modal frequencies are not provided here. The maximum BW in the gap-coupled design of proximity fed RMSA and C-shape MSAs is obtained for antenna parameters as, $C_h = 5.0$, $C_v = 10.3$, $W_c = 2.5$, $g = 0.75$, $L = 8.6$, $W = 4.5$, $h_a = 2.4$, $h_s = 2.3$, $x_f = 2.5$, $L_f = 1.3$ cm, and their results are provided in Fig. 2(a). The simulated and measured BWs for the gap-coupled antenna are 743 MHz (57.3%) and 752 MHz (58.43%), respectively. The antenna offers a broadside gain larger than 7 dBi over the complete S_{11} BW with a peak value close to 8 dBi. The surface current distributions at TM_{10} mode on RMSA and TM_{20} mode on C-shape MSAs are shown in Figs. 2(b) and (c). At the two modes which contribute

to the BW, surface currents are directed along the horizontal direction. This gives broadside radiation pattern across the S_{11} BW with cross polar component of radiation lower than 15 dB as compared with the co-polar component of radiation level. The dimensions of C-shape MSAs on the two sides of RMSA are same, thus parasitic patch frequencies are identical. This achieves symmetric radiation pattern across the S_{11} BW.

To increase the BW further, similar to the reported gap-coupled designs, additional resonators lying in the vicinity of fed RMSA can be added, but this will increase the antenna size. In the present work, resonant modes are added in the structure without considering additional parasitic elements. To achieve this, the initial tuning of higher order modes of fed RMSA or C-shape MSAs is considered. While the higher order modes are tuned, the polarization of additional modes needs to be the same as that of modes of RMSA and gap-coupled C-shape patches which contribute to the BW. Thus, to explore the higher order modes in the gap-coupled design, impedance behavior of gap-coupled antenna is studied over a higher frequency range as shown in Fig. 2(e). The next resonant mode observed in the impedance curve is TM_{02} mode on the fed RMSA, as confirmed from its surface current distribution provided in Fig. 2(d). The tuning of this mode in addition to the reorientation of surface current components along the patch length is achieved by adding a pair of rectangular slots in the RMSA leading to the design of an E-shape MSA, as shown in Fig. 1(a). The pair of slots, which realizes the E-shape structure tunes the TM_{02} mode frequency on RMSA with respect to TM_{10} and TM_{20} modes to yield maximum possible BW as shown in Fig. 2(e). With the slots, the polarization of modified TM_{02} mode is along the patch length as shown in Fig. 1(c). The parametric optimization process for E-shape MSA is well described in the literature [26, 27], hence not discussed here. The optimum results are obtained for antenna parameters as, $C_h = 5.0$, $C_v = 10.3$, $W_c = 2.5$, $g = 0.75$, $L = 8.6$, $W = 4.5$, $L_s = 2.7$, $W_s = 0.4$, $y = 2.0$, $h_a = 2.6$, $h_s = 2.2$, $x_f = -2.7$, $L_f = 1.9$ cm, and their results are given in Fig. 3. The proximity feed position x_f is present on the other side of the patch central point as shown in Fig. 1, hence the value mentioned is negative. This feed position ensures optimum coupling to the resonant modes present for the maximum BW [27].

For $S_{11} \leq -10$ dB, the BW observed in the simulation is 902 MHz (66.13%), and that in the measurement is 925 MHz (67.84%). The antenna offers a broadside gain of more than 7 dBi across the BW with a peak value larger than 8 dBi. The radiation pattern across the S_{11} BW is in the broadside direction with E-plane aligned along $\Phi = 0^0$. The cross polar component of radiation is lower than 10 dB as compared with the co-polar radiation level over a complete S_{11} BW thereby ensuring LP response. The experimental setup to measure the S_{11} BW is mentioned in Fig. 3(b).

To increase the BW further, additional slots can be cut inside the E-shape MSA. However, the optimization process becomes difficult as multiple resonant modes are involved in the same radiating patch. Hence, optimizing the impedance at modified modes together is then a complex procedure. Also because of the geometry of C-shape MSA, its higher order modes are in higher frequency range. Further, they do not have the same E-field polarization as against the modes present in the gap-coupled design. Therefore, a new method is adapted here that involves the placement of a printed resonant rectangular loop outside the boundaries of the E-shape MSA. Thus, a gap-coupled design of E-shape MSA with C-shape MSAs and loaded with printed rectangular loop resonator is shown in Fig. 1(a). The rectangular loop is placed on the other side of the substrate and below the E-shape MSA. A detailed dimensional description of the resonant loop structure is provided in Fig. 4(a). The lengths 'R_1' and 'R_2' form the horizontal and vertical lengths of the rectangular loop, whereas the position 'P' is from the patch center point. W_r is the width of the rectangular loop, which remains the same in its horizontal and vertical sections. The parametric study was carried out to analyze the effects of the resonant mode introduced by the rectangular loop structure, and the resonance curve plots for the variation in 'P' and 'R_1' & 'R_2' are shown in Figs. 4(b) and (c).

With the addition of printed rectangular loop, resonant mode distribution of the gap-coupled antenna changes. Surface current distributions at the observed resonant modes for $P = 1.9$, $R_1 = 3.7$, $R_2 = 1.6$ cm are provided in Figs. 5(a)–(d). The first two modes correspond to TM_{10} mode in E-shape MSA and TM_{20} mode in C-shape patch. The fourth mode corresponds to the modified TM_{02} mode in E-shape patch. As noted from the surface current distribution at third mode shown in Fig. 5(c), surface currents exhibit two half-wavelength variations over a rectangular loop length. Hence, corresponding mode is referred to as TM_{20r}. Here 'r' represents the mode on printed rectangular loop. For this current distribution, the polarization of TM_{20r} mode is along horizontal direction as shown in Fig. 1(c). As currents are circulating over the entire vertical and horizontal section of the rectangular loop, changes in rectangular loop dimensions R_1 and R_2 alter its resonance frequency. This effect is confirmed from their resonance curve plots shown. This reduction in frequency holds true for the increase in R_1 or R_2, with other dimensions remaining constant. With the variation in 'P', the mutual coupling is changed between resonant modes on the patch and the printed loop. It was observed in the parametric study that, when the rectangular loop is placed below and near the pair of slots in E-shape MSA, i.e., left side of the patch center, the coupling to the resonant loop is not observed, and the relevant resonant peak is absent. The coupling is present only when the rectangular loop is present on the right side, i.e., away from the pair of slots. As per the current distribution for the loop resonant mode, maximum field is present towards the open circuit edges of the printed rectangular loop. For the loop orientation as shown in Fig. 1(a), when the loop is placed below the pair of slots, the maximum resonant field (open circuit edge) on E-shape patch coincides with the minimum field point on the loop, which results in poor gap-coupling. Against this when printed rectangular loop is placed on the other side of proximity feed or the pair of slots, the position of maximum of fields on E-shape patch and printed rectangular loop matches that result in stronger coupling between the two. Hence, in the optimum design, the position of rectangular loop is present on the other side of the pair of slots. Thus, by employing a rectangular printed loop without altering the frequencies of the E-

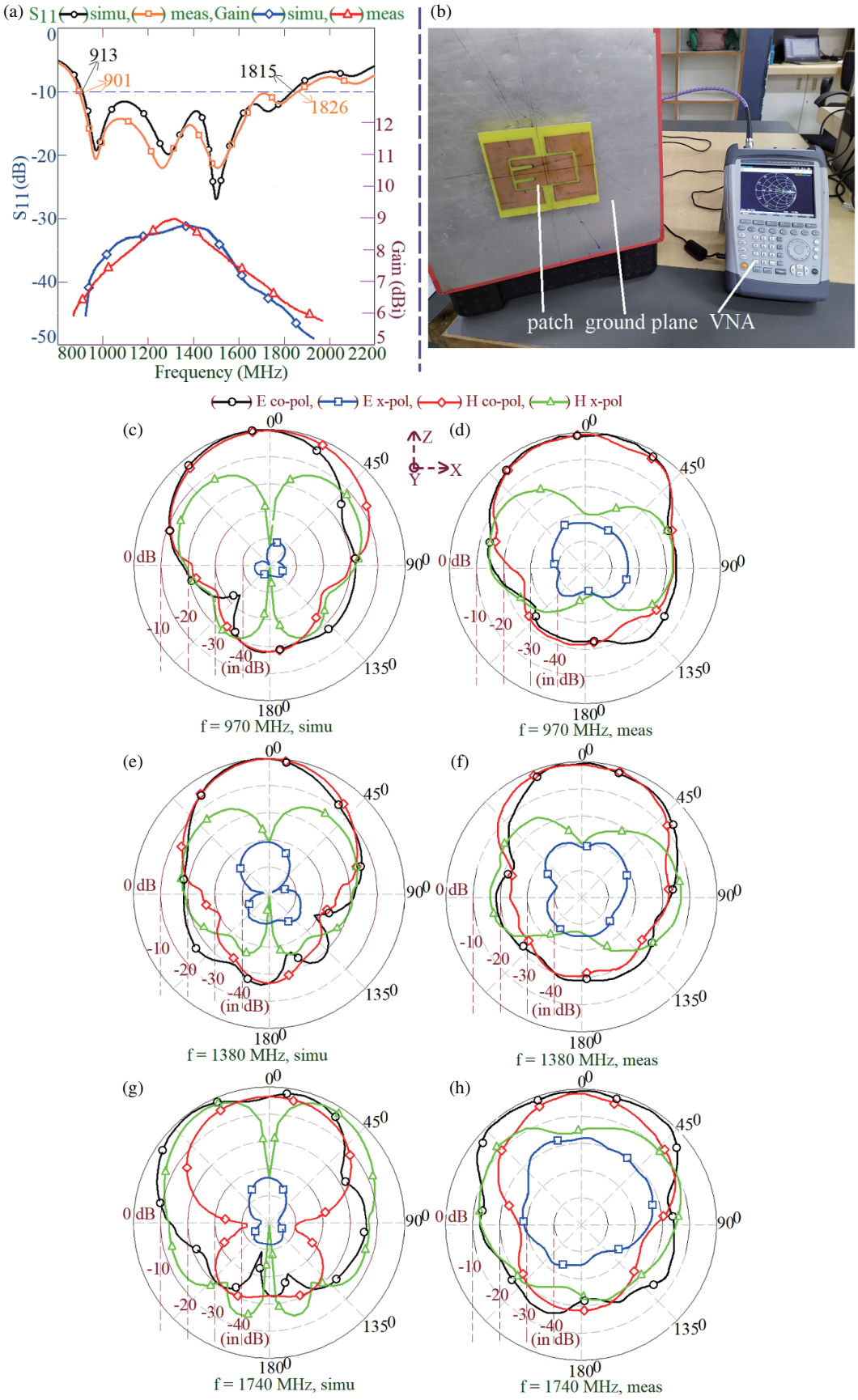

FIGURE 3. (a) S_{11} BW and gain plots, (b) S_{11} BW measurement setup, (c)–(h) radiation pattern plots over the BW for gap-coupled variation of proximity fed E-shape MSA with C-shape MSAs.

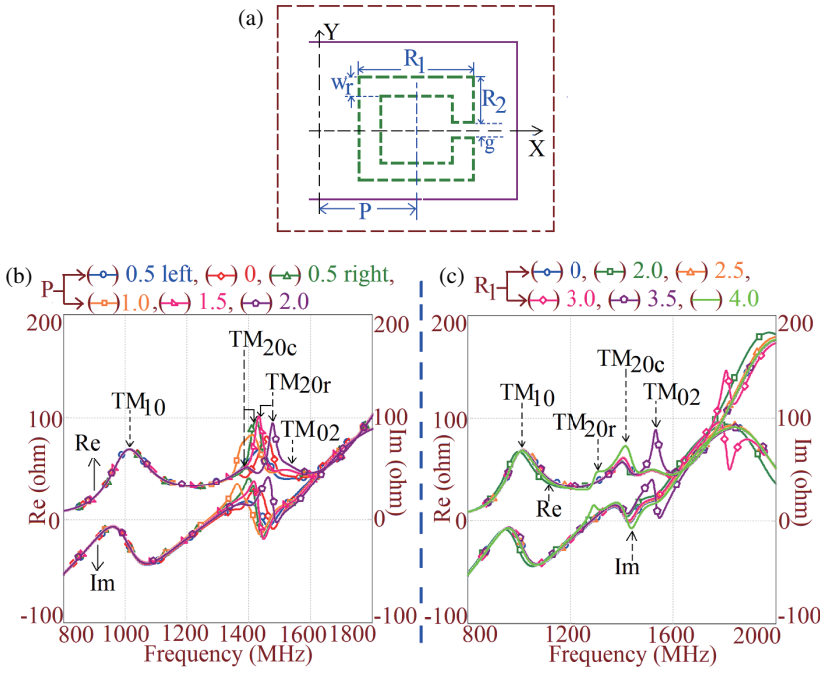

FIGURE 4. (a) Dimensional representation of rectangular resonant loop placed below the E-shape patch and its resonance curve plots for variation in (b) 'P', (c) 'R_1'.

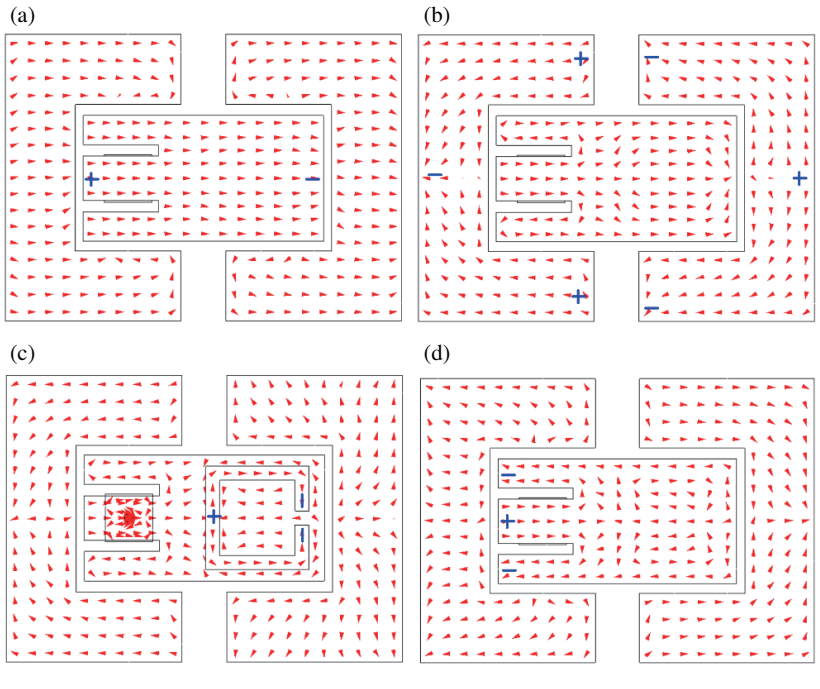

FIGURE 5. Surface current distribution at (a) TM_{10} mode in E-shape MSA, (b) TM_{20} mode in C-shape MSA, (c) TM_{20r} mode in printed rectangular loop and (d) TM_{02} mode in E-shape MSA. (a) $f_{10} = 1012$ MHz, (b) $f_{20c} = 1388$ MHz, (c) $f_{20r} = 1454$ MHz, (d) $f_{02} = 1542$ MHz.

shape and C-shape patch modes, additional resonant mode is introduced that enhances the BW.

Using the parametric optimization for 'P' and 'R_1' & 'R_2', an optimum response is realized, and the antenna dimensions for the same are, $P = 1.9$, $R_1 = 3.7$, $R2 = 1.6$, $g = wr = 0.5$, $L_f = 1.7$, $x_f = -2.7$, $h_s = 2.2$ cm. The simulated and measured BWs for $S_{11} \leq -10$ dB are 945 MHz (68.1%) and 969 MHz (69.83%), respectively as shown in Fig. 6(a). The antenna offers the broadside gain of more than 7 dBi over the S_{11} BW with maximum value larger than 8 dBi. The S_{11} BW measurement setup and the fabricated antenna are given in Fig. 6(b). The radiation pattern across the S_{11} BW, as shown

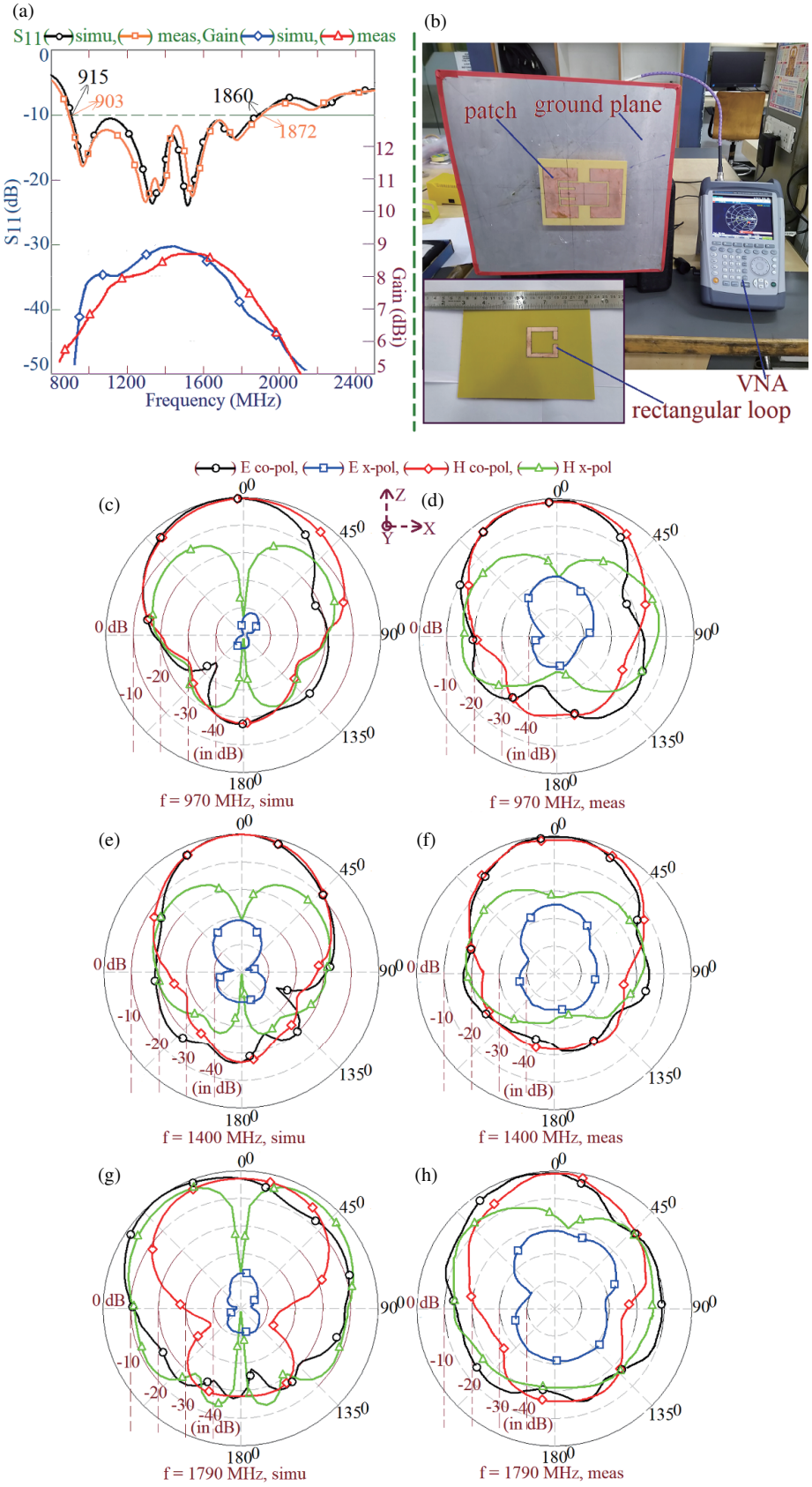

FIGURE 6. (a) S_{11} BW and gain plots (b) S_{11} BW measurement setup, (c)–(h) radiation pattern plots over the BW for gap-coupled variation of proximity fed E-shape MSA with C-shape MSAs loaded with printed rectangular loop.

FIGURE 7. Radiation pattern and gain measurement setup.

in Figs. 6(c)–(h), is in the broadside direction with E-plane aligned along $\Phi = 0^0$. The cross polar component of radiation is lower than 10 dB as compared with the co-polar radiation level over complete BW thereby ensuring LP response. In the proposed gap-coupled designs, towards the higher frequencies of the BW, MSA gain decreases to around 7 dBi. The reduction in the gain towards the higher frequencies of BW is attributed to the modified TM_{02} mode on E-shape MSA and TM_{20r} mode on the resonant loop structure, which is placed below the fed patch. Due to these two modes, vertical contribution of surface currents is excited on the patch that reduces the broadside gain towards those frequencies. However, over the complete bandwidth it remains above 6–7 dBi, which is an appreciably large value from the practical applications. Radiation pattern and gain are measured inside the antenna laboratory as shown in Fig. 7. Reference wideband high gain horn antennas were used in the measurement. A minimum far-field distance is maintained between the antenna under test (AUT) and the horn antenna.

The far-field distance is calculated with respect to the highest frequency of measurement. To achieve a better accuracy in the lab measurement, three-antenna method is used in the gain measurement. Thus, unlike the reported multi-resonator antennas wherein multiple additional resonators are used to increase the BW, in this work while using a single pair of parasitic resonators and by exploiting the resonant modes of the fed patch and resonator lying beneath it, BW of the gap-coupled antenna is increased. With these additional resonators, antenna size is not further increased.

3. DESIGNING METHODOLOGY FOR WIDEBAND GAP-COUPLED VARIATION OF E-SHAPE MSA

The gap-coupled design of E-shape MSA with two C-shape patches loaded with a resonant printed rectangular loop yields optimum result for BW and gain. For this wideband design, this section presents a design methodology to realize a similar gap-coupled antenna in a different frequency range. Initially based on the above wideband design, resonant length formulations at all the resonant modes are presented. To formulate the length, variations in the surface current directions against the variation in respective patch and slot parameters are extensively studied. The resonant length at TM_{10} mode in proximity fed RMSA is obtained by using Equation (1), and the frequency is calculated using (2). Here, h_t represents the total substrate thickness that equals $h + h_a$. The effective dielectric constant (ε_{re}) is calculated by using Equation (3). For RMSA of dimension, $L = 8.6$, $W = 4.5$, $h_a = 2.4$, $h = 0.16$ cm on FR4 substrate, the frequency calculated using (2) is 1195 MHz that matches closely with the simulated frequency of 1201 MHz. The antenna dimensions mentioned in various equations below are in cm, and the frequency calculated using them is in GHz.

$$L_e = L + 2\,(0.7h_t) \tag{1}$$

$$f_{10} = {}^{30}\!/_{2L_e\sqrt{\varepsilon_{re}}} \tag{2}$$

$$\varepsilon_{re} = \frac{\varepsilon_r\,(h + h_a)}{h + h_a\varepsilon_r} \tag{3}$$

For the gap-coupled C-shape patch, the resonant length formulation at TM_{20} mode (L_{20c}) is given by using Equation (4). In this equation, C_h and C_v are C-shape patch horizontal and vertical lengths, respectively, whereas W_c is the C-shape patch width as mentioned in Fig. 1(a). This equation considers the effective current path length along the center of the patch as shown in Fig. 8(a). The resonance frequency is calculated by using Equation (5) for the effective dielectric constant value as calculated by using Equation (3). For the C-shape MSA dimensions as, $C_h = 6.3$, $C_v = 10.3$, $W_c = 2.5$, $h_a = 2.6$, $h = 0.16$ cm, the calculated frequency using (5) is 1360 MHz. This agrees closely with the simulated frequency of 1366 MHz, as observed in the optimum gap-coupled design of C-shape patches with E-shape MSA.

$$L_{20c} = 2C_h + C_v - 2w_c \tag{4}$$

$$f_{20c} = {}^{30}\!/_{L_{20c}\sqrt{\varepsilon_{re}}} \tag{5}$$

The resonant mode currents on printed rectangular loop exhibit two half wavelength variation along the total length. In this case, the effective resonant length is obtained by taking the average of lengths L_1 and L_2 as mentioned in Fig. 8(b). Therefore, with reference to the dimensions shown in Fig. 4(a), effective resonant length at TM_{20} mode in printed rectangular loop is obtained by using Equations (6)–(8). The frequency is calculated by using Equation (9). ε_{re1} is the effective dielectric constant for the resonant printed rectangular loop and is calculated by using Equation (10). The printed rectangular loop is fabricated below the patch and on the other side of the FR4 substrate. Considering the fringing fields originating from the top and bottom side of the loop, some contribution of the fields is present between the loop and E-shape patch, as shown in Fig. 8(e). The Fringing fields see an effective dielectric constant as a dielectric constant of the dielectric medium, i.e., ε_r. Some percentage of the fringing fields pass through the top dielectric then through the air before terminating on the ground plane as mentioned in Fig. 8(e). These fields see the effective dielectric constant as that of the suspended dielectric substrate above the ground plane using finite air gap, i.e., ε_{re}. Since the

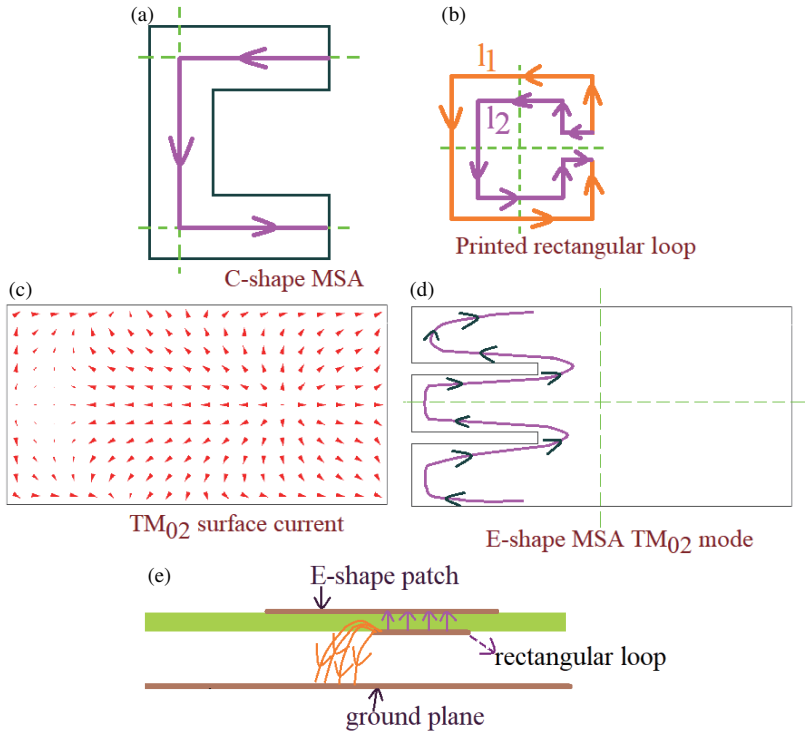

FIGURE 8. Surface current path for (a) C-shape MSA, (b) printed rectangular loop, (c), (d) TM_{02} mode current on E-shape MSA, (e) fringing field distribution for printed rectangular resonator loop.

fringing fields come across two different effective values of dielectric constant on two sides, attributed to the patch on one side and ground plane on the other, effective dielectric constant value for the rectangular loop mode is the average value, as mentioned in (10). For the rectangular strip and substrate dimensions as, $R_1 = 3.7$, $R_2 = 1.6$, $g = 0.5$, $W_r = 0.5$, $h_a = 2.6$, $h = 0.16$ cm, the frequency calculated using Equation (9) is 1433 MHz, which agrees closely with the simulated frequency of 1412 MHz.

$$l_1 = 2R_1 + 4R_2 + g \tag{6}$$

$$l_2 = 2R_1 + 4R_2 + g - 6w_r \tag{7}$$

$$L_{20r} = {}^{(l_1 + l_2)}/_{2} \tag{8}$$

$$f_{20r} = {}^{30}/_{L_{20r}\sqrt{\varepsilon_{re1}}} \tag{9}$$

$$\varepsilon_{re1} = {}^{(\varepsilon_r + \varepsilon_{re})}/_{2} \tag{10}$$

The surface current distribution at TM_{02} mode in proximity fed RMSA is shown in Fig. 8(c). At this resonant mode, surface currents are expected to be directed along patch width. However, there seems to be a variation along the patch length as well. This is attributed to the patch length being almost double in dimension against the width. As mentioned above, this dimensional ratio between length and width is primarily selected for the compact size. Because of this variation in currents along patch length, the formulation in effective patch width at TM_{02} mode is obtained by using Equation (11), and frequency is calculated by using Equation (12). The calculated frequency is 2460 MHz against the simulated frequency of 2420 MHz.

$$W_e = W + 1.2h_t + \left({}^{L}/_{2}\right) \tag{11}$$

$$f_{02} = {}^{30}/_{W_{e02}\sqrt{\varepsilon_{re}}} \tag{12}$$

The pair of slots in E-shape patch perturbs the surface current length at TM_{02} mode as shown in Fig. 8(d). The effect of slot is formulated as given in Equation (13). The surface currents at modified TM_{02} mode are circulating around the pair of slot lengths, and their effects are accounted by the fourth term on right hand side of Equation (13). The modified frequency is calculated by using Equation (12) for $W_{e02} = W_{e02s}$. The frequency calculated using Equation (12) is 1710 MHz against the simulated value of 1702 MHz as observed in the optimum gap-coupled design of E-shape MSA with C-shape patches, loaded with printed rectangular loop resonator. Thus, at all the resonant mode frequencies which contribute to the S_{11} BW, close prediction in their values using the proposed formulation is obtained. Using these formulations, the design methodology to realize similar wideband antenna is presented.

$$W_{e02s} = W + 1.2h_t + \left({}^{L}/_{2}\right) + \left({}^{1.5l_s}/_{L}\right)(4l_s) \tag{13}$$

The design methodology is initiated by specifying the band start frequency (f_{st}) of the S_{11} BW. In addition to the resonant length formulations given above, frequency and dimensional relations exist amongst the resonant modes, and antenna parameters of above optimum gap-coupled design are used in

the design methodology here. For the given f_{st}, TM_{10} mode frequency of proximity fed RMSA is calculated by using the relation mentioned in (14). The total substrate thickness for the antenna is calculated by using Equations (15) and (16). For calculating the wavelength in the air suspended dielectric at TM_{10} mode, the value of ε_{re} is unknown, as h_a is not available. Hence, an initial approximation of $\varepsilon_{re} = 1.05$ is considered. This approximation holds good as substrate thickness is more than $0.08\lambda_g$.

$$f_{10} = 1.311 f_{st} \tag{14}$$

$$\lambda_{g10} = {}^{30}/_{f_{10}\sqrt{\varepsilon_{re}}} \tag{15}$$

$$h_t = 0.113\lambda_{g10} \tag{16}$$

From the calculated value of h_t, the value of h_a is selected that is practically realizable as well as an integer number. Using this value and for FR4 substrate, ε_{re} and λ_{g10} are recalculated using Equations (3) and (15), respectively, and they are used in all further calculations. The RMSA length at the calculated TM_{10} mode frequency is obtained by using Equation (17), and further RMSA width is selected as $W = 0.523L$.

$$L = \left({}^{30}/_{2f_{10}\sqrt{\varepsilon_{re}}}\right) - 1.4h_t \tag{17}$$

As identified from the resonance curve plots for the optimum design of E-shape MSA gap-coupled with C-shape patch and rectangular resonant loop, TM_{20} mode frequency on C-shape patch bears a frequency ratio, $f_{20c} = 1.493 f_{st}$, with reference to the band start frequency of the BW. Using this relation, resonant length at C-shape patch mode is obtained using Equation (18). In the design of C-shape patch, three dimensions of the patch are present, i.e., C_v, C_h, and W_c. The resonance frequency in C-shape patch is governed by each of these parameters. Hence to simplify the process, a similar design of C-shape MSA in terms of patch dimension ratio as that selected in the above mentioned design is considered. Thus, respective lengths in C-shape MSA are selected as $C_h = 0.612C_v$, $W_c = 0.243C_v$. Using these relations and further by rearranging Equation (4), C-shape MSA vertical length C_v is calculated as mentioned in (19). Using this value of C_v, other C-shape patch dimensions are calculated. The amount of gap-coupling between the fed and parasitic patches is a function of substrate thickness and the frequency. Hence, air gaps g_c and g_x, as mentioned in Fig. 1(a), are taken as $0.109h_t$ and $0.58h_t$, respectively.

$$L_c = {}^{30}/_{f_{20c}\sqrt{\varepsilon_{re}}} \tag{18}$$

$$C_v = {}^{(L_c - 1.3h_t)}/_{1.738} \tag{19}$$

The resonant mode due to the printed rectangular loop resonator bears a frequency ratio, $f_{20r} = 1.543 f_{st}$, with reference to the band start frequency of the BW. Using this relation, resonant length (L_{20r}) at the rectangular loop mode is calculated as given in Equation (20). As mentioned in Equations (6)–(9), l_r depends upon R_1, R_2, g, and w_r. To simplify the process, dimensional relations like $R_1 = 2.3125R_2$, $g = 0.2135R_2$, $w_r = 0.3125R_2$ are used. Using this and by rearranging the terms on the two sides of Equation (8), effective resonant length is expressed in terms of one of the rectangular loop dimensions, as given in Equation (21). The effective dielectric constant for rectangular loop mode is calculated using Equation (10). Thus, using Equations (20)–(21) and above dimension relations for the rectangular loop, dimensions of the loop are calculated.

$$L_{20r} = {}^{30}/_{f_{20r}\sqrt{\varepsilon_{re}}} \tag{20}$$

$$R_2 = {}^{L_{20r}}/_{8} \tag{21}$$

The modified TM_{02} resonant mode of the E-shape MSA bears a frequency ratio, $f_{02s} = 1.86 f_{st}$, with reference to the band start frequency of the BW. Using it, effective RMSA width, which includes the effects of pair of rectangular slots, is calculated as mentioned in Equation (22). By using Equation (23), a pair of slot length L_s is obtained. This equation is obtained by rearranging the terms on the two sides of Equation (13) and expressing the same for L_s. Further, slot width W_s and separation between the pair of slots (y) is selected as $0.148L_s$ and 0.444 W, respectively. The proximity feed parameters are selected as $x_f = 0.111\lambda_{g10}$, $L_f = 0.07\lambda_{g10}$, $h_s = 0.07\lambda_{g10}$.

$$W_{02es} = {}^{30}/_{f_{02s}\sqrt{\varepsilon_{re}}} \tag{22}$$

$$l_s = \sqrt{\left({}^{L}/_{6}\right)\left(W_{02es} - W - \left({}^{L}/_{2}\right) - 1.2h_t\right)} \tag{23}$$

Using the above methodology, the gap-coupled design of proximity fed E-shape MSA with two C-shape MSAs and loaded with printed rectangular loop resonator is designed for $f_{st} = 1100$ MHz, and various antenna parameters calculated using above procedure are $h_a = 2.1$, $h = 0.16$, $L = 6.9$, $W = 3.6$, $L_s = 2.3$, $W_s = 0.3$, $y = 1.8$, $L_f = 1.4$, $x_f = 2.0$, $h_s = 1.8$, $C_v = 8.5$, $C_h = 5.2$, $W_c = 2.1$, $g_c = 0.3$, $g_x = 1.3$, $R_1 = 3.1$, $R_2 = 1.35$, $W_r = g = 0.4$ cm. The antenna simulated for these parameters and response is experimentally verified. The redesigned antenna offers simulated and measured BWs for $S_{11} \leq -10$ dB of 1190 MHz (69.06%) and 1207 MHz (69.11%), respectively. The antenna offers broadside radiation pattern across the complete BW with a peak gain larger than 8 dBi. The start frequency of the S_{11} BW is found to be 1128 MHz, which is closer to the initially selected frequency. This validates the design methodology for the proposed configuration. The BW and gain plots for the redesigned antenna are similar in nature to the original gap-coupled design discussed above. Hence to avoid the repeatability, results for redesigned antenna are not shown again. In the presented design methodology, in some of the antenna parameters mentioned above, calculated values are observed to be a non-integer number, which are rounded off to the nearest possible integer or practically realizable value. Hence in some of the cases, optimum results show deviation from the expected ones. In such cases, minor parametric optimization can be employed to realize the optimum BW.

4. RESULTS DISCUSSION AND COMPARATIVE ANALYSIS

The gap-coupled design of E-shape MSA with two C-shape MSAs and printed rectangular resonant loop yields maximum

TABLE 1. Comparison for the proposed wideband MSA against the reported configurations.

MSA shown in	Broadband Technique Used	Meas. BW (MHz,%)	Peak Gain (dBi)	h/λ_c	A/λ_c (in cm)
Figs. 1(a), (b)	Gap-coupled, slot cut	969, 69.84	9	0.13	6.7
Ref. [6]	Gap-coupled	52, 4.52	—	0.005	2.63
Ref. [7]	Gap-coupled	1200, 12.3	12	0.105	11.535
Ref. [8]	Gap-coupled	—, 6.3	—	0.068	4.84
Ref. [9]	Shorted MSA	730, 13.18	9.7	0.054	2.84
Ref. [10]	Parasitic patches, shorting post	810, 13.8	5.0	0.067	2.371
Ref. [11]	Parasitic patches, shorting post	270, 5.2	4.25	0.042	1.5
Ref. [12]	Shorting post, differential feed	20, 1.6	3.1	0.053	0.98
Ref. [13]	Gap-coupled, shorting post	6300, 40	10	0.113	1.35
Ref. [14]	Gap-coupled, shorting post	660, 11.5	7.07	0.042	3.76
Ref. [15]	Gap-coupled, slot, aperture coupling	2340, 41.1	10.0	0.142	>8
Ref. [16]	Gap-coupled, differential feeding	2020, 38.4	7.5	0.113	8.06
Ref. [17]	Gap-coupled, stacked	1114, 55.7	12.3	0.155	14.7
Ref. [18]	Modified patch geometry	350, 6.8	7	0.04	0.741
Ref. [19]	Gap-coupled	1500, 27.3	6.4	0.061	1.2
Ref. [20]	Gap-coupled, U-slot cut fed patch	1440, 26.2	8.5	0.115	2.78
Ref. [21]	Gap-coupled	835, 58.12	8.8	0.125	4.7
Ref. [22]	Gap-coupled	490, 20.04	9.5	0.053	10.77
Ref. [23]	Rectangular slots	880, 39.82	7.0	0.08	3.1
Ref. [24]	Double U-slot	2040, 68	10	0.023	2.224
Ref. [25]	U-slot, AMC layer	2920, 58.6	12.1	0.07	22
Ref. [26]	Rectangular slots	408, 24.82	7.2	0.076	3.74
Ref. [28]	Modified patch shape, slots, shorting post, differential feed	1110, 29.4	9.9	0.079	12.8
Ref. [29]	Modified patch shape, slots, shorting post, differential feed	620, 26.5	9.9	0.05	6.653
Ref. [30]	Rectangular slots, modified printed element	80, 9	7	0.04	5.4
Ref. [31]	Modified patch shape, slots, slot cut ground	1960, 30.1	8.0	0.054	2.542
Ref. [32]	Gap-coupled, parasitic strips	728, 55	9	0.115	5.2

BW and a peak gain. Therefore, to present the technical novelty in the proposed work, detailed comparison of the proposed work against the reported wideband configurations is presented in Table 1. In the comparison, wideband designs obtained using multi-resonator configurations, resonant slot cut designs, MSAs loaded with a shorting post, modified patch shape configurations and slot cut ground plane designs have been considered. The reported configurations selected in the comparison are optimized in different frequency bands as well as on different substrate thicknesses. Therefore, a normalized total patch size and substrate thickness in terms of the guided wavelength (λ_c) at the center frequency of S_{11} BW are considered in Table 1 for the comparison.

The gap-coupled design consisting of multiple resonators does offer nearly 5% BW on a thinner substrate, but the realized gain is small as design is optimized on a thinner lossy substrate [6, 8]. The gap-coupled patch antenna presented in [7] offers large gain, but patch size is large attributed to the offset placed sectoral patches. The MSAs discussed in [9–12] employ shorting post, multiple resonators in the form of shorted para-

sitic patches, and a differential feeding. Those designs offer lower BW than the proposed configuration. The gap-coupled design discussed in [13] optimized in 15 GHz spectrum employs multiple shorted patches gap-coupled with a coaxially fed rectangular patch. Here in spite of multiple resonators present, S_{11} BW is only 40% on an electrically thicker substrate. The gap-coupled design presented in [14] employs parasitic shorted microstrip line feeding gap-coupled with the fed patch. It offers lower BW and gain than the proposed design. Further design guidelines for the shorted microstrip line that adds to the BW are not discussed. The gap-coupled design discussed in [15] offers BW $>$ 40% with a peak gain of 10 dBi. However, it employs aperture coupling method which is complex in implementation. Further, the total antenna dimensions are large. The differentially fed wideband design discussed in [16] requires large antenna size as against the proposed optimum configuration. The wideband design discussed in [17] employs parasitic patches in the planar as well as stacked layer. They do offer substantially higher BW and gain, but overall antenna dimension is large. The modified patch shape design discussed in [18] does have smaller antenna volume, but the realized BW and gain are also smaller. The wideband designs discussed in [19–22, 32] employs multiple resonators which are placed in the vacant space around the fed patch. The designs discussed in [19, 20, 22] offer lower BW than the proposed optimum design. The wideband designs discussed in [21, 32] does offer higher BW and gain, but they employ three to four parasitic resonator pairs, thus increasing the design complexity. The wideband multiple slots loaded design discussed in [23] offers smaller S_{11} BW whereas the wideband thinner substrate design presented in [24] employs differential feeding and offers endfire radiation characteristics. The U-slot cut rectangular patch design offers wideband response with higher gain, attributed to the used AMC layer [25], but this design requires large antenna size. The modified patch shape designs discussed in [28, 29] use the combination of modified shape of the geometry, shorting post, rectangular slot, and differential feeding, but still they offer BW less than 30% with higher patch size. A technique to achieve a wideband response on a thinner substrate while considering the slot cut design is presented in [30]. This design offers BW less than 10%. Further detailed guideline to design printed circuit element which helps in achieving this wideband response on a thinner substrate is not presented. The modified ground plane design discussed in [31] employs modifications in the patch as well as the ground plane. In spite of these multiple modifications in the antenna geometry, obtained BW is smaller. Further, with the realized modifications in patch and ground plane, which of the resonant modes that contribute to the BW is not discussed.

In contrast to the reported configurations, the proposed design initially employs simpler gap-coupled technique for the BW enhancement, in which the design is restricted to one pair of parasitic resonators, which are placed around the vacant space of the fed patch. Further additional resonators are added in the structure first by using a pair of rectangular slots which realizes wideband E-shape configuration, and further loading the structure with a printed resonant loop that lies beneath the patch. Thus unlike the reported configurations that consider adding multiple resonators around the fed patch or stacked layer, present configuration employs different methods for adding multiple resonators which yields BW improvement. Although multiple resonant modes in the form of parasitic patch, modes introduced by slots and rectangular loop are present, the proposed study outlines the design methodology that helps in realizing similar wideband configuration in different frequency bands, which can match as per the given wireless application. Thus novelty in the proposed configuration lies first in utilizing simpler gap-coupling technique for BW enhancement and further utilizing novel techniques to add multiple resonant modes which does not add to the antenna size increment. The optimum gap-coupled design offers BW close to 70% with a peak gain of larger than 8 dBi. Hence, considering all the antenna parameters together proposed configuration provides optimum result for S_{11} BW, gain against the antenna volume, while considering all methods of BW improvements.

5. CONCLUSIONS

The proximity fed gap-coupled design of E-shape MSA with parasitic C-shape MSAs and loaded with resonant printed rectangular loop is presented. The wideband response is attributed to the optimum inter-spacing between the TM_{10} mode of RMSA with reference to the TM_{20} mode on C-shape MSAs and rectangular loop and modified TM_{02} mode of the fed RMSA. The proposed work utilizes the vacant space around the fed patch for BW improvement as well as utilizes the slots and resonators placed beneath the fed patch, thus limiting the increase in antenna size while considering gap-coupled technique. The optimum design achieves S_{11} BW of nearly 70% with a peak broadside gain larger than 8 dBi. The design methodology is put forward which helps in realizing similar configurations in different frequency bands as per the given wireless application.

REFERENCES

[1] Kumar, G. and K. P. Ray, *Broadband Microstrip Antennas*, Artech House, 2002.

[2] Wong, K.-L., *Compact and Broadband Microstrip Antennas*, John Wiley & Sons, 2004.

[3] Kovitz, J. M. and Y. Rahmat-Samii, "Using thick substrates and capacitive probe compensation to enhance the bandwidth of traditional CP patch antennas," *IEEE Transactions on Antennas and Propagation*, Vol. 62, No. 10, 4970–4979, 2014.

[4] Herscovici, N., "A wide-band single-layer patch antenna," *IEEE Transactions on Antennas and Propagation*, Vol. 46, No. 4, 471–474, 1998.

[5] Kumar, G. and K. Gupta, "Nonradiating edges and four edges gap-coupled multiple resonator broad-band microstrip antennas," *IEEE Transactions on Antennas and Propagation*, Vol. 33, No. 2, 173–178, 1985.

[6] Aanandan, C. K., P. Mohanan, and K. G. Nair, "Broad-band gap coupled microstrip antenna," *IEEE Transactions on Antennas and Propagation*, Vol. 38, No. 10, 1581–1586, 1990.

[7] Kandwal, A. and S. K. Khah, "A novel design of gap-coupled sectoral patch antenna," *IEEE Antennas and Wireless Propagation Letters*, Vol. 12, 674–677, 2013.

[8] Balaji, U., "Bandwidth enhanced circular and annular ring sectoral patch antennas," *Progress In Electromagnetics Research Letters*, Vol. 84, 67–73, 2019.

[9] Wang, Z., J. Liu, and Y. Long, "A simple wide-bandwidth and high-gain microstrip patch antenna with both sides shorted," *IEEE Antennas and Wireless Propagation Letters*, Vol. 18, No. 6, 1144–1148, 2019.

[10] Xu, K. D., H. Xu, Y. Liu, J. Li, and Q. H. Liu, "Microstrip patch antennas with multiple parasitic patches and shorting vias for bandwidth enhancement," *IEEE Access*, Vol. 6, 11 624–11 633, 2018.

[11] Ou, J.-H., S.-W. Dong, J. Huang, X. Y. Zhang, W. Che, and Q. Xue, "A compact microstrip antenna with extended half-power beamwidth and harmonic suppression," *IEEE Transactions on Antennas and Propagation*, Vol. 68, No. 6, 4312–4319, 2020.

[12] Sun, C., "A design of low profile microstrip patch antenna with bandwidth enhancement," *IEEE Access*, Vol. 8, 181 988–181 997, 2020.

[13] Cao, Y., Y. Cai, W. Cao, B. Xi, Z. Qian, T. Wu, and L. Zhu, "Broadband and high-gain microstrip patch antenna loaded with parasitic mushroom-type structure," *IEEE Antennas and Wireless Propagation Letters*, Vol. 18, No. 7, 1405–1409, 2019.

[14] Rathod, S. M., R. N. Awale, K. P. Ray, and A. D. Chaudhari, "Broadband gap-coupled half-hexagonal microstrip antenna fed by microstrip-line resonator," *International Journal of RF and Microwave Computer-Aided Engineering*, Vol. 28, No. 6, e21273, 2018.

[15] Sun, W., Y. Li, Z. Zhang, and Z. Feng, "Broadband and low-profile microstrip antenna using strip-slot hybrid structure," *IEEE Antennas and Wireless Propagation Letters*, Vol. 16, 3118–3121, 2017.

[16] Cheng, B., Z. Du, and D. Huang, "A differentially fed broadband multimode microstrip antenna," *IEEE Antennas and Wireless Propagation Letters*, Vol. 19, No. 5, 771–775, 2020.

[17] Chopra, R. and G. Kumar, "Broadband and high gain multilayer multiresonator elliptical microstrip antenna," *IET Microwaves, Antennas & Propagation*, Vol. 14, No. 8, 821–829, 2020.

[18] Yoo, J.-U. and H.-W. Son, "A simple compact wideband microstrip antenna consisting of three staggered patches," *IEEE Antennas and Wireless Propagation Letters*, Vol. 19, No. 12, 2038–2042, 2020.

[19] Wi, S.-H., Y.-S. Lee, and J.-G. Yook, "Wideband microstrip patch antenna with U-shaped parasitic elements," *IEEE Transactions on Antennas and Propagation*, Vol. 55, No. 4, 1196–1199, 2007.

[20] Lu, H.-X., F. Liu, M. Su, and Y.-A. Liu, "Design and analysis of wideband U-slot patch antenna with U-shaped parasitic elements," *International Journal of RF and Microwave Computer-Aided Engineering*, Vol. 28, No. 2, e21202, 2018.

[21] Chavali, V. A. P. and A. A. Deshmukh, "Wideband designs of proximity fed isosceles triangular microstrip antennas gap-coupled with parasitic pairs of sectoral patches," *International Journal of RF and Microwave Computer-Aided Engineering*, Vol. 32, No. 6, e23132, 2022.

[22] Yang, D., H. Zhai, C. Guo, and H. Li, "A compact single-layer wideband microstrip antenna with filtering performance," *IEEE Antennas and Wireless Propagation Letters*, Vol. 19, No. 5, 801–805, 2020.

[23] Li, W.-W., Q.-H. Li, Y. Meng, J.-Y. Wang, and W.-M. Xu, "A broadband microstrip patch antenna with multiple open slots," *Microwave and Optical Technology Letters*, Vol. 61, No. 3, 626–632, 2019.

[24] Radavaram, S. and M. Pour, "Wideband radiation reconfigurable microstrip patch antenna loaded with two inverted U-slots," *IEEE Transactions on Antennas and Propagation*, Vol. 67, No. 3, 1501–1508, 2018.

[25] De Dieu Ntawangaheza, J., L. Sun, C. Yang, Y. Pang, and G. Rushingabigwi, "Thin-profile wideband and high-gain microstrip patch antenna on a modified AMC," *IEEE Antennas and Wireless Propagation Letters*, Vol. 18, No. 12, 2518–2522, 2019.

[26] Wong, K.-L. and W.-H. Hsu, "A broad-band rectangular patch antenna with a pair of wide slits," *IEEE Transactions on Antennas and Propagation*, Vol. 49, No. 9, 1345–1347, 2001.

[27] Deshmukh, A. A. and K. P. Ray, "Analysis of broadband Psi (Ψ)-shaped microstrip antennas," *IEEE Antennas and Propagation Magazine*, Vol. 55, No. 2, 107–123, 2013.

[28] Feng, S., L. Zhang, Z. Weng, and Y.-C. Jiao, "A wideband differential-fed microstrip patch antenna based on quad-mode resonance with radiation patterns correction," *IEEE Transactions on Antennas and Propagation*, Vol. 71, No. 6, 5404–5409, 2023.

[29] Liu, X., W. Hu, S. Gao, L. Wen, Q. Luo, R. Xu, and Y. Liu, "A wideband triple-mode differentially fed microstrip patch antenna," *IEEE Antennas and Wireless Propagation Letters*, Vol. 20, No. 7, 1160–1164, 2021.

[30] Chen, Y., S. Yang, and Z. Nie, "Bandwidth enhancement method for low profile E-shaped microstrip patch antennas," *IEEE Transactions on Antennas and Propagation*, Vol. 58, No. 7, 2442–2447, 2010.

[31] Mondal, K. and P. P. Sarkar, "Gain and bandwidth enhancement of microstrip patch antenna for WiMAX and WLAN applications," *IETE Journal of Research*, Vol. 67, No. 5, 726–734, 2021.

[32] Chavali, V. A. P. and A. A. Deshmukh, "Multi-resonator variations of circular microstrip antenna with narrow annular sectoral patches for wideband response," *Progress In Electromagnetics Research C*, Vol. 114, 143–158, 2021.

[33] CST Microwave Studio, Version 2019.